Applied Physics Letters

Anomalous multi-ramp fractional vortex beams with arbitrary topological charge jumps

Cite as: Appl. Phys. Lett. **117**, 241103 (2020); https://doi.org/10.1063/5.0028490
Submitted: 04 September 2020 . Accepted: 08 December 2020 . Published Online: 17 December 2020

Jun Zeng, Hao Zhang, Zhiheng Xu, Chengliang Zhao, Yangjian Cai, and Greg Gbur

Applied Physics Letters ARTICLE scitation.org/journal/apl

Anomalous multi-ramp fractional vortex beams with arbitrary topological charge jumps

Cite as: Appl. Phys. Lett. **117**, 241103 (2020); doi: 10.1063/5.0028490
Submitted: 4 September 2020 · Accepted: 8 December 2020 ·
Published Online: 17 December 2020

Jun Zeng,[1,2,3] Hao Zhang,[2] Zhiheng Xu,[1] Chengliang Zhao,[2,a)] Yangjian Cai,[1,2,a)] and Greg Gbur[3,a)]

AFFILIATIONS

[1]Shandong Provincial Engineering and Technical Center of Light Manipulations and Shandong Provincial Key Laboratory of Optics and Photonic Device, School of Physics and Electronics, Shandong Normal University, Jinan 250014, China
[2]School of Physical Science and Technology, Soochow University, Suzhou 215006, China
[3]Department of Physics and Optical Science, The University of North Carolina at Charlotte, Charlotte, North Carolina 28223, USA

[a)]**Authors to whom correspondence should be addressed:** zhaochengliang@suda.edu.cn; yangjiancai@suda.edu.cn; and gjgbur@uncc.edu

ABSTRACT

Traditional fractional vortex beams are well-known "jump" beams: that is, their net topological charge jumps by unity as the effective topological charge of the source passes a half-integer value. Here, we propose an anomalous multi-ramp fractional vortex (AMRFV) beam. Unlike the traditional fractional vortex beams, an AMRFV beam can be designed to have arbitrary jumps in topological charge at any critical threshold of the source charge. We walk through some examples of AMRFV beams using simulations and present a clear interpretation of the multi-jump characteristic based on the evolution of phase singularities.

The study and application of beams with helical wavefronts and the associated singularity of phase at their core have become an important aspect of the field now known as *singular optics*.[1] In 1992, such vortex beams with an azimuthal order l were shown by Allen *et al.*[2] to possess an orbital angular momentum (OAM) of $l\hbar$ per photon. In fact, the phase in a counterclockwise path around every vortex in a general wavefield changes by $2\pi l$, where l is referred to as the topological charge (TC) of the vortex and always takes on an integer value. The discrete nature of topological charge has generated much interest in its use as an information carrier in optical communications,[3] among other applications.

Though the topological charge can only take on integer values, it is possible to formally generate a "fractional vortex beam" by the use of a fractional spiral phase plate that induces only a fraction of a 2π phase circulation around the beam axis. This was studied in detail by Berry in 2004[4] (though an early look at such possibilities appeared in 1995[5]) who also showed how the topological charge of a modified plane wave jumps by unity when the effective charge of the fractional plate takes on a half-integer value. This result was demonstrated experimentally soon after.[6] Since Berry's pioneering work, considerable attention has been paid to such fractional vortex beams, both coherent and partially coherent cases.[7–15] These studies show that the most obvious change induced by the introduction of fractional topological charges is to create a radial opening in the intensity distribution, which can be used to guide and transport particles.[7] In particular, unidirectional notch arrays formed by fractional vortex arrays have been used for particle sorting.[8]

Early work on fractional beams imagined creating them with a conventional spiral phase plate,[16] with a single adjustable spiral ramp in the azimuthal direction providing the fractional phase twist and an effective fractional topological charge at the source. However, in a demonstration that fractional vortex beams create new topological charge through a "Hilbert Hotel" mechanism, Gbur[17] showed that an adjustable multi-ramp spiral phase plate, with m ramps in the azimuthal direction instead of one, could create a jump of m in topological charge as the source charge is increased, corresponding to m rooms being simultaneously freed in Hilbert's Hotel. This hinted at the possibility that even more sophisticated fractional spiral phase plates could be designed, which generate an arbitrary jump of topological charge with an increase in the fractional source charge. It is reasonable to believe that the future requirements for vortex beams with the TC structure will develop toward diversity and richness, especially for particle trapping,[8] information security,[18] and optical communication.[19] For example, Ma *et al.*[20] realized optical vortex shaping with a controllable OAM distribution by introducing a phase jump factor, and Tkachenko *et al.*[21] realized a more uniform micro-manipulation by

evenly distributing the phase jump of a fractional vortex beam into multiple parts. Therefore, the generation and modulation of vortex beams with complex and diverse TC structures will be a topic of constant attention.

In this Letter, we modify the transmission function of the spiral phase plates from Ref. 17 to design an anomalous multi-ramp spiral phase plate (AMRSPP), which generates an anomalous multi-ramp fractional vortex (AMRFV) beam, and demonstrate its rich and varied TC jump characteristics with simulations. We show that it is possible to design a plate with a single tunable parameter—the effective source charge—that will have topological charge jumps of arbitrary size that appear in any order desired.

Figure 1 shows a designed AMRSPP involving three types of adjustable parameters, including the number of multi-ramp sections m, the input fractional topological charge α, and the fractional phase control coefficients $\beta_p (p = 0, 1, 2, \ldots, m-1)$ in each ramp section. The transmission function of an AMRSPP is then given by

$$T(\theta) = \exp\left[\frac{i\alpha(\theta - 2\pi p/m)}{\beta_p}\right], \quad \frac{2\pi p}{m} \le \theta < \frac{2\pi(p+1)}{m}, \tag{1}$$

where θ denotes the azimuthal angle.

In analogy with a conventional spiral phase plate, we envision the AMRSPP as a transparent plate with a polymer replicated on a glass substrate, and the thickness of each ramp section varies azimuthally. Here, the phase increases by $2\pi\alpha/m\beta_p$ in each ramp section, which is quite different from the simple design in Ref. 16 and that possessing the same phase change rate in each ramp section in Ref. 17. Using such an AMRSPP, we can attach a specific phase twist to the beam and generate an AMRFV beam with complex and diverse TC structures. When $m = 1$ and $\beta_0 = 1$, the model designed by Eq. (1) reduces to a conventional spiral phase plate, which is used to generate a traditional fractional vortex beam. For $m \ge 2$ and all $\beta_p = 1$, the model designed by Eq. (1) reduces to a multi-ramp spiral phase plate, which is used to realize a fractional vortex beam with a multi-unit (i.e., m-unit) TC jump.[17]

It is to be noted that we can generalize our spiral phase plate even further: the ramp sections can be taken to have different azimuthal widths, and the height of each ramp section can be taken to vary independently. Here, we primarily consider plates with a single variable parameter—the "source charge"—and demonstrate that we can create Hilbert Hotel style jumps of topological charge in any order and any degree even under this restricted case.

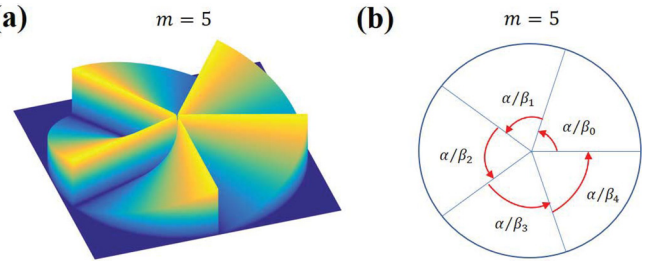

FIG. 1. (a) Illustration of an AMRSPP with $m = 5$ and (b) the top view of (a) with detailed structural distribution.

For mathematical convenience, we consider the illumination of such a phase plate by a normally incident plane wave. According to the Fresnel diffraction principle and the Collins formula,[22] the field of a monochromatic plane wave with unit amplitude passing through a spiral phase plate of integer topological charge n [designed to have a transmission function $T_0(\theta) = \exp(in\theta)$] is expressed as

$$E_n(\rho, \theta, z) = \sqrt{\frac{\pi\rho^2}{2}} \exp(ikz) \exp(in\theta) \exp(i\rho^2)(-i)^{|n|/2} \times \left[J_{\frac{|n|-1}{2}}(\rho^2) - iJ_{\frac{|n|+1}{2}}(\rho^2)\right], \tag{2}$$

with

$$\rho = \sqrt{\xi^2 + \eta^2}, \quad \xi = \sqrt{k/4z}x, \quad \text{and} \quad \eta = \sqrt{k/4z}y, \tag{3}$$

where z and $\boldsymbol{r} = (x, y)$ denote the distance from the phase plate and the transverse position vector in a plane of z, respectively. k is the wavenumber and ρ is the scaled dimensionless variable. $J_n(\cdot)$ denotes the nth order Bessel function of the first kind.

Following Berry[4] and Gbur,[17] the transmission function of the AMRSPP can be expanded into the Fourier series of integer order

$$T(\theta) = \sum_{n=-\infty}^{\infty} C_n \exp(in\theta), \tag{4}$$

with

$$C_n = \frac{1}{2\pi} \sum_{p=0}^{m-1} \frac{\exp(-i2\pi pn/m)}{i(\alpha/\beta_p - n)} \left\{ \exp\left[i\frac{2\pi}{m}\left(\frac{\alpha}{\beta_p} - n\right)\right] - 1 \right\}. \tag{5}$$

Thus, by applying Eq. (2), the field of an AMRFV beam can be obtained as follows:

$$E_\alpha(\rho, \theta, z) = \sum_{n=-\infty}^{\infty} C_n E_n(\rho, \theta, z). \tag{6}$$

This expression describes the field characteristics of an AMRFV beam of any fractional charge α and at any propagation distance z.

To study the topological behavior of AMRFV beams, we consider the net topological charge (also called total vortex strength) within a particular integral radius ρ_0, defined as[4]

$$t = \lim_{\rho \to \rho_0} \frac{1}{2\pi} \int_0^{2\pi} d\theta \cdot \frac{\partial}{\partial\theta} \arg[E_\alpha(\rho, \theta, z)] = \lim_{\rho \to \rho_0} \frac{1}{2\pi} \int_0^{2\pi} d\theta \cdot \mathrm{Re}\left\{-i \cdot \frac{\partial E_\alpha(\rho, \theta, z)/\partial\theta}{E_\alpha(\rho, \theta, z)}\right\}. \tag{7}$$

To illustrate the possibilities in controlling the TC jump in AMRFV beams, we limit our investigation to three special cases, $m = 5$, $m = 6$, and $m = 7$, and consider how the net topological charge depends on the other beam parameters, namely, α and β_p.

Figure 2 shows how the jump in topological charge depends on the choice of the fractional phase control coefficients β_p. From the figure, it is clear that the topological charge jumps at values of α such that

$$\alpha = 0.5(2j - 1)m\beta_p \quad (j = 1, 2, 3, \ldots), \tag{8}$$

for every value of p, where j is a positive integer and denotes the cycle ordinal. Obviously, the emergence of the jump has certain periodic

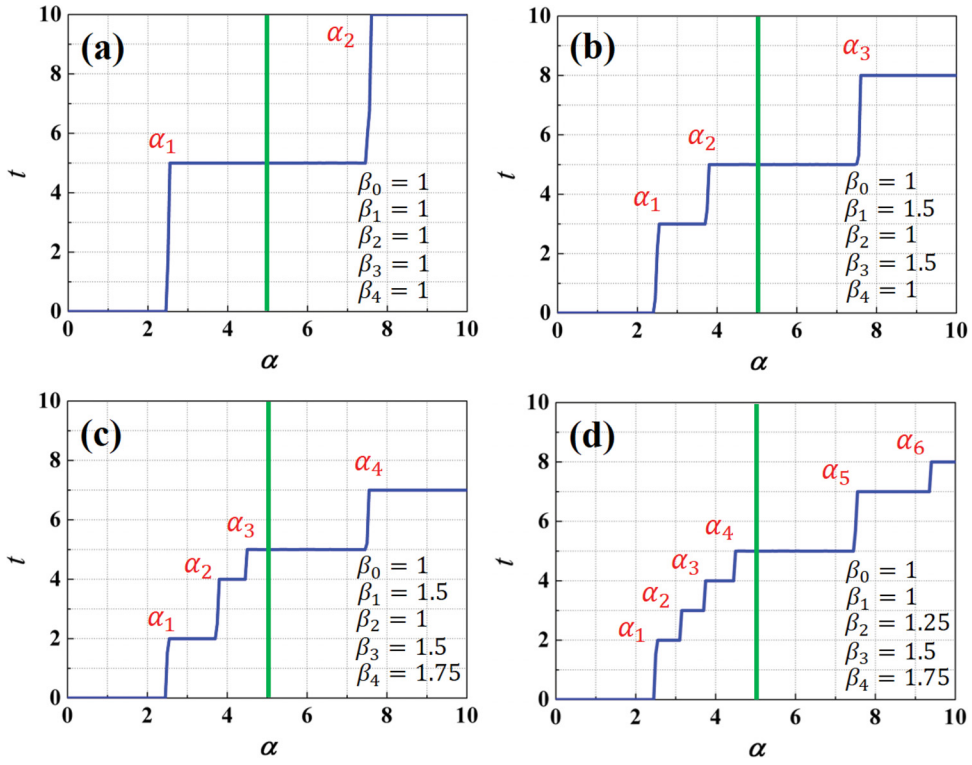

FIG. 2. Net topological charge t of an AMRFV beam as a function of α with different fractional phase control coefficients β_p for $m = 5$, calculated by numerically evaluating the integral of Eq. (7) with $\rho_0 = 20$. (a) One distinct phase control coefficient, (b) two coefficients, (c) three coefficients, and (d) four coefficients.

characteristics. It is to be noted that this periodicity is not always symmetrical (simply repeating the previous cycle), and the specific periodicity is determined by the values of β_p and m. For example, Fig. 2(a) is a typical repeatable cycle and the period is 5, while Figs. 2(b)–2(d) are not. To give a clear and quantifiable description, we only focus on the situation in the first period (e.g., $0 \le \alpha \le 5$) below, and the cases in other periods (larger α) can be deduced by analogy. In the first period (i.e., the left side of the green line), the number of distinct jumps that occur and the size of each jump are equal to the number of different values of β_p and the multiplicity of β_p, respectively. The number of different values of β_p, for instance, in Figs. 2(a)–2(d) are 1 (i.e., 1), 2 (i.e., 1 and 1.5), 3 (i.e., 1, 1.5, and 1.75), and 4 (i.e., 1, 1.25, 1.5, and 1.75), respectively. Thus, the number of jumps that occur are 1, 2, 3, and 4, respectively. For Fig. 2(a), there are five identical values of β_p, and so the single jump unit is 5 (which occurs at $\alpha_1 = 2.5$). For Fig. 2(b), the multiplicities of $\beta_p = 1$ and $\beta_p = 1.5$ are 3 and 2, respectively; thus, the first jump amount (at $\alpha_1 = 2.5$) is 3 and the second jump amount (at $\alpha_2 = 3.75$) is 2. In a similar fashion, α_1–α_3 in Fig. 2(c) and α_1–α_4 in Fig. 2(d), as well as the jump amounts, can be determined.

Figure 3 shows how the topological charge jump can be adjusted by adjusting the number m of multi-ramp sections. Comparing Figs. 2(b) and 3, we find that although both figures have only two values of β_p (i.e., 1 and 1.5), the choice of different m leads to different jump locations and different jump units.

From Figs. 2 and 3, it can be concluded that

$$t = \sum_{p=0}^{m-1} \mathrm{Int}\left[\frac{\alpha}{m\beta_p} + \frac{1}{2}\right], \tag{9}$$

where Int denotes the integer arithmetic. This formula is surprisingly straightforward and makes it relatively easy to choose the number of ramps m and the values β_p to produce any evolution of topological charge desired.

The means by which the topological charge jumps may be seen to be a Hilbert Hotel evolution of the number of singularities in the system, as first noted in Ref. 17. In Fig. 4, we calculate the phase evolution of an AMRFV beam with the same parameters as in Fig. 2(c). An optical vortex is represented by a point where all the colors converge—a singularity of phase. Left- and right-handed vortices (corresponding to positive and negative TCs) are represented by the phase increasing or decreasing in a counterclockwise path around the singularity, respectively.

As α increases from zero to $\alpha_1 = 0.5m\beta_0 = 2.5$, pairs of vortices with equal and opposite TCs begin to appear, with additional pairs appearing along two lines extending away from the origin [Fig. 4(a)]. These pairs contribute nothing to the net topological charge t, which remains $t = 0$. For $\alpha = \alpha_1 = 2.5$, two infinite lines of vortex pairs (labeled ① and ②) have appeared, corresponding to the two values $\beta_0 = \beta_2 = 1$, as seen in Fig. 4(b). As α increases past $\alpha = \alpha_1 = 2.5$, the negatively charged vortices annihilate with their more distant positive neighbor, leaving the net topological charge $t = 2$ [Fig. 4(c)]. At the same time, two new finite vortex chains (i.e., ③ and ④) begin to grow due to

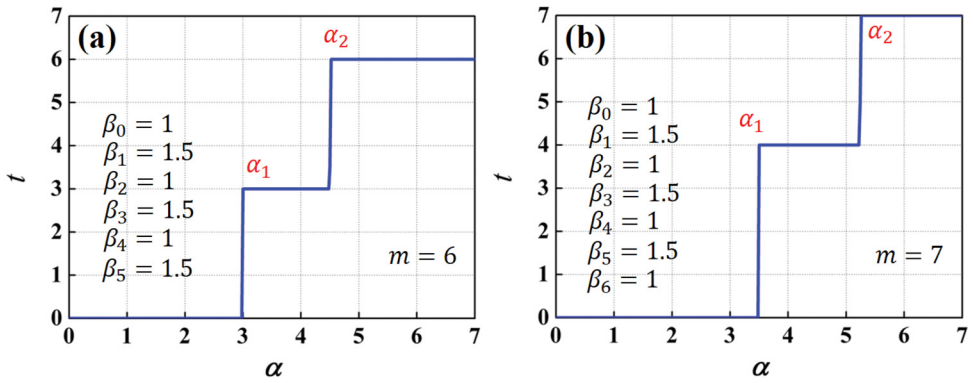

FIG. 3. Net topological charge t of an AMRFV beam as a function of α with different m for $\rho_0 = 20$. (a) Six ramp sections and (b) seven ramp sections.

the two values $\beta_1 = \beta_3 = 1.5$ [Fig. 4(d)]. As α increases from $\alpha_2 = 0.5m\beta_1 = 3.75$ to $\alpha_3 = 0.5m\beta_4 = 4.375$ [Fig. 4(e)], vortex chains ③ and ④ contribute two vortices with positive TC and we finally have $t = 4$. Again during the annihilation of vortex chains ③ and ④, a new vortex chain ⑤ is created due to the ramp with $\beta_4 = 1.75$. Finally, as α increases past $\alpha = \alpha_3 = 4.375$ [Fig. 4(f)], all the annihilations are done and the net topological charge $t = 5$. Through the above analysis, we know that the evolution process in Fig. 4 is in complete agreement with that in Fig. 2(c) and Eq. (9).

More specifically, Eq. (9) can be further explained by the evolution of vortices, namely, as the equivalent TC α/β_p in each ramp section gradually approaches the values of $m/2$, a line of vortices in each ramp section is created, for instance, as can be seen in Figs. 4(a) and 4(b) for the evolution of the vortex chain ① or ②. After $\alpha/\beta_p = m/2$, we are left with an unbalanced vortex with positive TC in each corresponding ramp section, which leads to the TC jump, for instance, as can be seen in Fig. 4(d) for the remaining individual vortex after the annihilation of ① or ②.

Each discontinuity of an AMRSPP results in a corresponding line of low intensity along the radial direction that is most intense when Eq. (8) is satisfied, but which exists for a range of neighboring α values. AMRFV beams can, therefore, be designed to have any number of

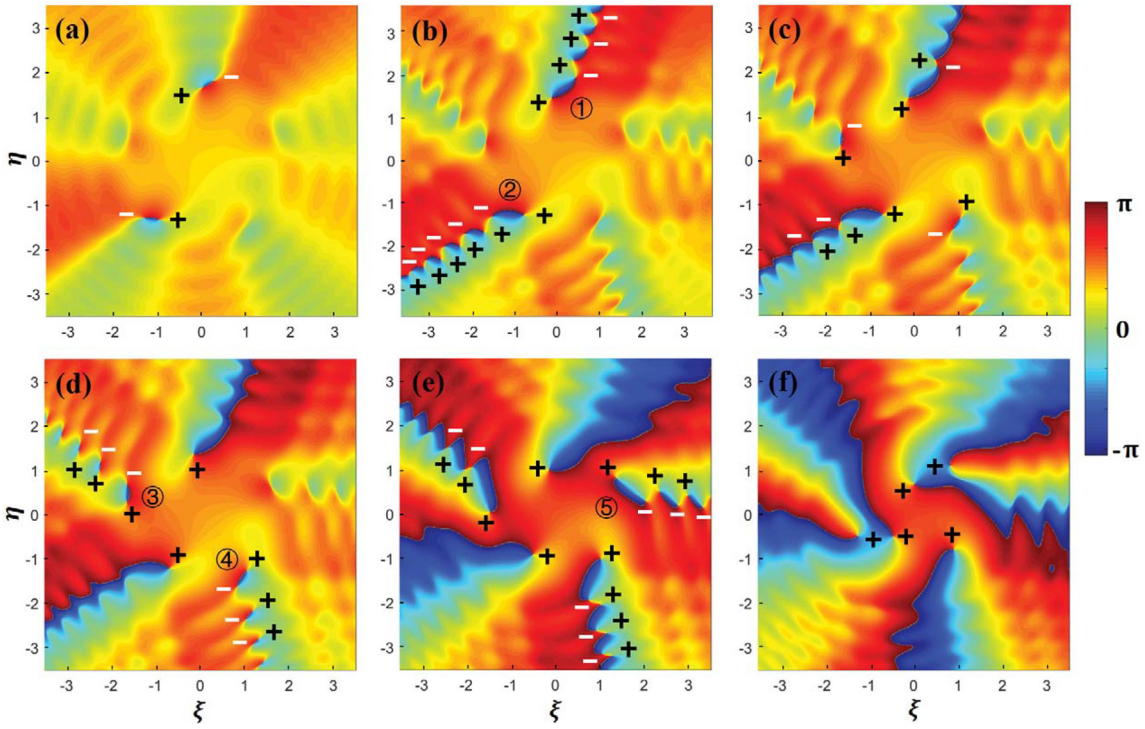

FIG. 4. Phase evolution of an AMRFV beam with $m = 5$ and $[\beta_0, \beta_1, \beta_2, \beta_3, \beta_4] = [1, 1.5, 1, 1.5, 1.75]$. The symbols "+"and "−" denote unit left- and right-handed vortices, respectively. (a) $\alpha = 1.99$, (b) $\alpha = 2.5$, (c) $\alpha = 2.75$, (d) $\alpha = 2.9$, (e) $\alpha = 4.3$, and (f) $\alpha = 5.8$.

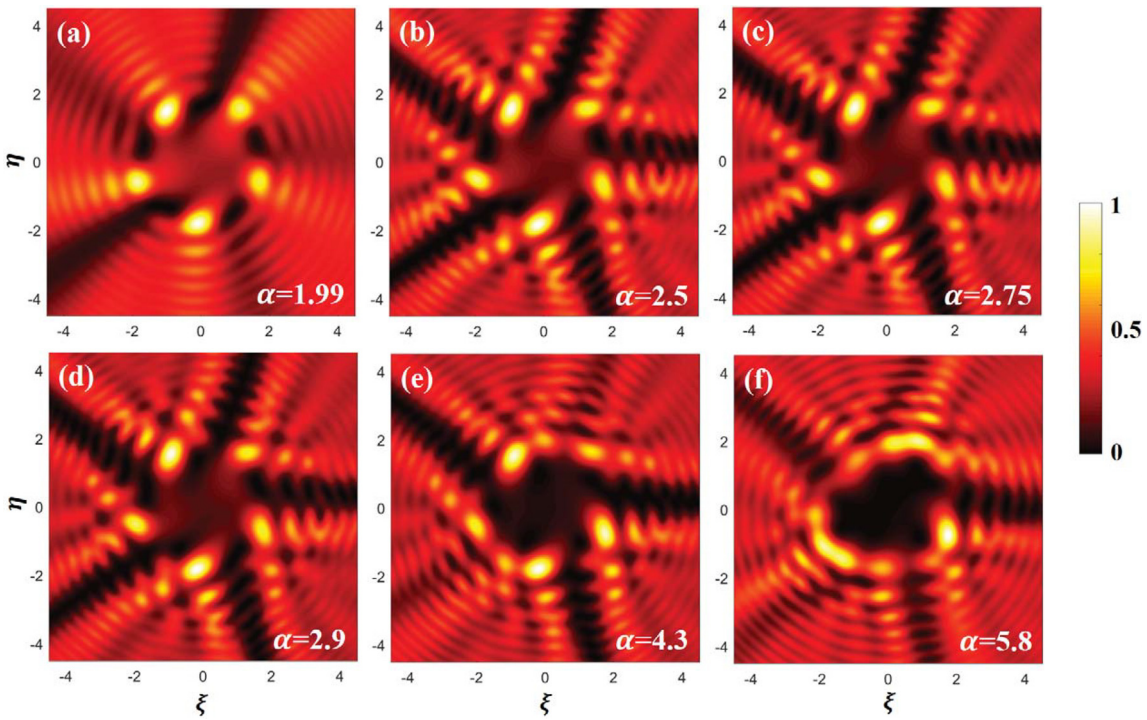

FIG. 5. Intensity evolution of an AMRFV beam with $m = 5$ and $[\beta_0, \beta_1, \beta_2, \beta_3, \beta_4] = [1, 1.5, 1, 1.5, 1.75]$. (a) $\alpha = 1.99$, (b) $\alpha = 2.5$, (c) $\alpha = 2.75$, (d) $\alpha = 2.9$, (e) $\alpha = 4.3$, and (f) $\alpha = 5.8$.

low-intensity "spokes" radiating out from the origin over particular ranges of α. This result is qualitatively different from the conventional fractional vortex beam[4] that possesses only one spoke. In Fig. 5, the intensity profiles corresponding to the phase profiles of Fig. 4 are shown. In Fig. 5(a), with $\alpha = 1.99$, there are two distinct low intensity spokes, arising from the influence of ramps $p = 0$ and $p = 2$, whereas for Figs. 5(b)–5(d) there are five spokes, as all ramps affect the intensity profile. In Fig. 5(e), α is large enough that the original two low-intensity spokes have vanished, leaving only the three corresponding to $p = 1$, 3, and 4. As α increases further, in Fig. 5(f), we can see that the two spokes corresponding to $p = 1$, 3 have started to diminish, leaving only the single spoke for $p = 4$.

It is to be noted that our results apply to an ideal plane wave or a beam that is effectively wide enough to be approximated as a plane wave. It has been shown recently for both traditional fractional vortex sources[12] and multi-ramp fractional vortex sources[23] that for narrow width beams, the jumps in topological charge occur at integer, and not half-integer, source values. The implications for AMRV beams of finite width will be considered in separate work.

It should be further noted that the infinite chain of vortices will not be seen in a practical experiment, due to the finite size of the beam. However, as seen theoretically in Ref. 17 and experimentally in Ref. 6, one will see an extended line of vortices, which will inevitably be lost in the darkness in the outskirts of the beam. It may be said that we see the "signature" of the infinite mathematics in the finite system.

The intensity profiles of AMRFV beams have been verified experimentally. The experimental setup for generating an AMRFV beam is shown in Fig. 6. After passing through a beam expander, the laser beam is modified using the phase mask displayed in a SLM. Then, the modified beam passes through a $4-f$ system and circular aperture, which only chooses the +1st order. The generated AMRFV beams are recorded by the CCD.

A comparison of the experimental intensity patterns and theoretical intensity patterns is shown in Fig. 7. Excellent agreement can be seen in the position of the darkest spokes, and good agreement in the

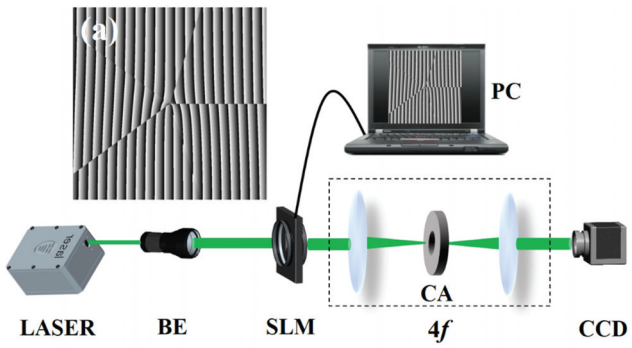

FIG. 6. Experimental setup for generating an AMRFV beam. (a) Phase mask written into the SLM. BE, beam expander; SLM, spatial light modulator; CA, circular aperture; 4f: $4-f$ system; and CCD, charge coupled device.

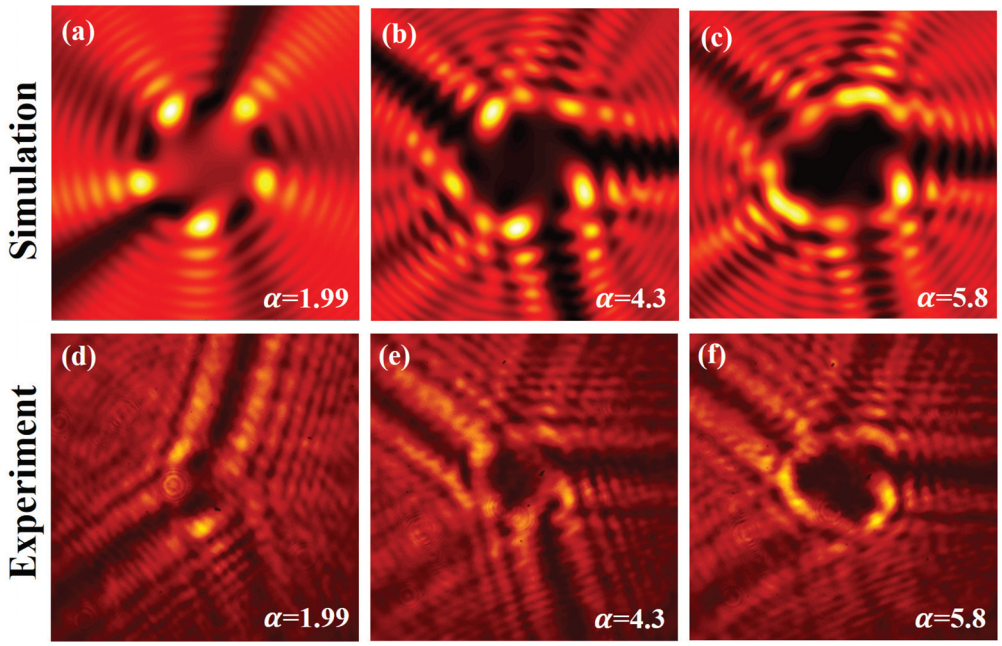

FIG. 7. A comparison between simulations (a)–(c) and experiments (d)–(f) of intensity patterns for AMRFV beams. The parameters are the same as those in Fig. 5.

shape of the beam core, indicating that our theoretical analysis is a reliable indicator of the actual intensity patterns produced in practice.

In this Letter, we have shown how even an optical element with a single tunable parameter can be used to generate rich topological behavior; if one considers an AMRSPP with m sections, each with an independently tunable ramp charge α_p, Eq. (9) can be generalized to the form

$$t = \sum_{p=0}^{m-1} \mathrm{Int}\left[\frac{\alpha_p}{m} + \frac{1}{2}\right]. \tag{10}$$

If we further allow the azimuthal width of the m sections to vary, with the constraint that the total equals 2π, it seems clear that we can then also adjust the azimuthal positions of the vortex chains, which will roughly coincide with the discontinuity lines between sections. By generalizing Eqs. (1)–(6) to take into account m azimuthal sections of width $2\pi/m_p$, we may further generalize Eq. (10) to the form

$$t = \sum_{p=0}^{m-1} \mathrm{Int}\left[\frac{\alpha_p}{m_p} + \frac{1}{2}\right]. \tag{11}$$

Both the azimuthal positions of the vortex chains, as well as their evolution as a function of α_p, will depend on the choice of m_p.

This Letter, therefore, shows that it is possible to generalize the Hilbert Hotel vortex creation of Ref. 17 through the use of an anomalous multi-ramp spiral phase plate, allowing an arbitrary number of vortices to be created at any value of the source charge α. These results show that we have great flexibility in controlling the topological charge of an AMRFV beam and can readily predict and plan the appearance of new vortices. We have revealed the relationships between the value where the jump appears, the number of jumps that occur, the unit of each jump of an AMRFV beam, and beam parameters.

Similar to the strategy discussed in Ref. 7, we foresee the application of the above low intensity spokes to trap, guide, and sort particles. Particles with a high refractive index tend to be drawn into high intensity regions due to the gradient force and low intensity regions serve effectively as a barrier. Because an AMRFV beam possesses multiple low-intensity spokes that can be designed to appear or disappear in any order, the spokes can be used to collect particles in different regions and then combine groups of particles in sequence. Several rotating AMRFV beams could be combined to make an assembly line of particle organization. Thus, compared with the conventional fractional vortex beam with single radial opening for single-particle trapping, an AMRFV beam possessing multiple low-intensity spokes has an advantage in the ability to simultaneously manipulate multiple particles.

In addition to the aforementioned applications, the diversity of TC jumps can greatly improve the information capacity of quantum information systems and makes a new OAM multiplication/division functional transformation integrated device possible.[24] Thus, our work may be useful in multi-particle trapping, quantum computing, and optical device manufacturing and highlights the richness of possibilities in vortex creation.

AUTHORS' CONTRIBUTIONS

The authors contributed equally to this work.

This work was supported by the National Key Research and Development Program of China (No. 2019YFA0705000), National Natural Science Foundation of China (NSFC) (Nos. 91750201, 11525418, 11974218, and 11774250), Local Science and Technology

Development Project of the Central Government (No. YDZX20203700001766), Innovation Group of Jinan (No. 2018GXRC010); China Scholarship Council (No. 201906920047), and Tang Scholar. Greg Gbur was financially supported by the Office of Naval Research of America (No. MURI N00014-20-1-2558).

DATA AVAILABILITY

The data that support the findings of this study are available from the corresponding author upon reasonable request.

REFERENCES

[1]G. J. Gbur, *Singular Optics* (CRC Press, Boca Raton, 2017).
[2]L. Allen, M. W. Beijersbergen, R. J. C. Spreeuw, and J. P. Woerdman, Phys. Rev. A **45**, 8185 (1992).
[3]G. Gbur and R. K. Tyson, J. Opt. Soc. Am. A **25**, 225 (2008).
[4]M. V. Berry, J. Opt. A **6**, 259 (2004).
[5]I. V. Basistiy, M. S. Soskin, and M. V. Vasnetsov, Opt. Commun. **119**, 604 (1995).
[6]J. Leach, E. Yao, and M. J. Padgett, New J. Phys. **6**, 71 (2004).
[7]S. Tao, X. C. Yuan, J. Lin, X. Peng, and H. Niu, Opt. Express **13**, 7726 (2005).
[8]C. Guo, Y. Yu, and Z. Hong, Opt. Commun. **283**, 1889 (2010).
[9]Y. Fang, Q. Lu, X. Wang, W. Zhang, and L. Chen, Phys. Rev. A **95**, 023821 (2017).
[10]J. Zeng, X. Liu, F. Wang, C. Zhao, and Y. Cai, Opt. Express **26**, 26830 (2018).
[11]S. Li, B. Shen, X. Zhang, Z. Bu, and W. Gong, Opt. Express **26**, 23460 (2018).
[12]J. Wen, L. Wang, X. Yang, J. Zhang, and S. Zhu, Opt. Express **27**, 5893 (2019).
[13]J. Zeng, C. Liang, H. Wang, F. Wang, C. Zhao, G. Gbur, and Y. Cai, Opt. Express **28**, 11493 (2020).
[14]Y. Yang, X. Zhu, J. Zeng, X. Lu, C. Zhao, and Y. Cai, Nanophotonics **7**, 677 (2018).
[15]H. Wang, L. Liu, C. Zhou, J. Xu, M. Zhang, S. Teng, and Y. Cai, Nanophotonics **8**, 317 (2019).
[16]M. Beijersbergen, R. Coerwinkel, M. Kristensen, and J. Woerdman, Opt. Commun. **112**, 321 (1994).
[17]G. Gbur, Optica **3**, 222 (2016).
[18]X. Fang, H. Ren, and M. Gu, Nat. Photonics **14**, 102 (2020).
[19]Y. Ren, Z. Wang, P. Liao, L. Li, G. Xie, H. Huang, Z. Zhao, Y. Yan, N. Ahmed, A. Willner *et al.*, Opt. Lett. **41**, 622 (2016).
[20]H. Ma, X. Li, H. Zhang, J. Tang, H. Li, M. Tang, J. Wang, and Y. Cai, Opt. Lett. **44**, 1379 (2019).
[21]G. Tkachenko, M. Chen, K. Dholakia, and M. Mazilu, Optica **4**, 330 (2017).
[22]S. Wang and D. Zhao, *Matrix Optics* (CHEP-Springer, Beijing, 2000).
[23]J. Wen, B. Gao, G. Zhu, Y. Cheng, S. Zhu, and L. Wang, Opt. Laser Technol. **131**, 106411 (2020).
[24]Y. Wen, I. Chremmos, Y. Chen, Y. Zhang, and S. Yu, Phys. Rev. Lett **124**, 213901 (2020).